Astronomy
&
Astrophysics

Dynamical rearrangement of super-Earths during disk dispersal

II. Assessment of the magnetospheric rebound model for planet formation scenarios

Beibei Liu and Chris W. Ormel

Anton Pannekoek Institute (API), University of Amsterdam, Science Park 904, 1090GE Amsterdam, The Netherlands
e-mail: [b.liu;c.w.ormel]@uva.nl

ABSTRACT

Context. The *Kepler* mission has provided a large sample to statistically analyze the orbital properties of the super-Earth planet population. We hypothesize that these planets formed early and consider the problem of matching planet formation theory to the current orbital configurations. Two scenarios – disk migration and in-situ formation – have been proposed to explain the origin of these planets. In the migration scenario, planets migrate inward to the inner disk due to planet-disk interaction, whereas in the in-situ scenario planets assemble locally. Therefore, planets formed by migration are expected to end up in resonances, whereas those formed in-situ are expected to stay in short period ratios and in non-resonant orbits. Both predictions are at odds with observations.
Aims. We investigate whether a preferred formation scenario can be identified through a comparison between the magnetospheric rebound model and the *Kepler* data.
Methods. We conduct N-body simulations of two-planet systems during the disk dispersal phase. Several distributions of model parameters are considered and we make a statistical comparison between the simulations and the *Kepler* observations.
Results. Comparing the migration and the in-situ scenarios, we find that magnetospheric rebound tends to erase the difference in the orbital configuration that was initially presented. After disk dispersal, not all planets are in resonance in the migration scenario, whereas planets do not remain in compact configurations in the in-situ scenario. In both scenarios, the orbits of planets increase with the cavity expansion, and their period ratios have a wider distribution.
Conclusions. From a statistical perspective, the magnetospheric rebound model reproduces several observed properties of *Kepler* planets, such as the fact that a significant number of planets are not in resonances and planet pairs can end up at large period ratios. The disparity in orbital configuration between the two formation scenarios is substantially reduced after disk dispersal.

Key words. planet-disk interactions – planets and satellites: formation

1. Introduction

The *Kepler* and K2 missions have vastly increased the number of detected planets and revolutionized our understanding of planet formation. One of the most intriguing findings is that super-Earths (defined here as radii $R_p \leq 4 R_\oplus$ with orbital periods $P \lesssim 100$ days) are the most abundant type of planets. Since the *Kepler* mission has discovered so many super-Earth planets, the dynamical configuration of these planets can be analyzed from a statistical perspective.

We summarize here the key properties of super-Earths (see Winn & Fabrycky 2015, for a review). First, super Earths are very common. The occurrence of super-Earths among solar-type stars is around 50% (Petigura et al. 2013) with a slight dependence on stellar type (Howard et al. 2012; Fressin et al. 2013; Mulders et al. 2015), but independent of stellar metallicity (Wang & Fischer 2015; Buchhave et al. 2014). These findings are also consistent with ground-based radial velocity surveys (Mayor et al. 2011; Bonfils et al. 2013). Second, super-Earths are commonly discovered in multiple, compact, and short period systems with relatively low eccentricities and inclinations (Fang & Margot 2012; Johansen et al. 2012; Fabrycky et al. 2014; Van Eylen & Albrecht 2015; Shabram et al. 2016; Xie et al. 2016). Third, the distribution of their period ratios is neither strongly peaked at resonances, nor entirely uniformly spaced (Fabrycky et al. 2012). Fourth, some super-Earth are

inferred to contain H/He-rich envelopes. We can deduce the composition of a few dozen *Kepler* super-Earth planets from transit-timing variation (Lithwick et al. 2012) or RV follow-up surveys (Marcy et al. 2014). The bulk densities of many of these planets are too low to be consistent with a purely rocky (Earth-like) composition. Detailed modeling of mass-radius relationships indicates that these super-Earths contain non-negligible H/He envelopes (Lopez & Fortney 2014). They may have already formed in the early gas-rich disk phase, and also do not suffer violent giant-impacts after the depletion of disk gas (Inamdar & Schlichting 2015).

For the solar system, local formation models (see Raymond et al. 2014; Morbidelli & Raymond 2016, for reviews and references therein) attempt to explain the origin of terrestrial planets. These models are formulated according to the minimum-mass solar nebula (MMSN) profile for the surface density (Weidenschilling 1977b; Hayashi 1981). Extending the local formation paradigm to extrasolar systems, the minimum-mass extrasolar nebula (MMEN) disk model has been constructed (Chiang & Laughlin 2013). However, Σ_{MMEN} is much larger than Σ_{MMSN}, approximately by a factor 10. Apart from the large disk mass, the surface density profiles of MMENs are inconsistent with sub-millimeter observations of the outer disks around young T Tauri stars (Andrews et al. 2009; Raymond & Cossou 2014). In addition, Schlichting (2014)

demonstrated that for many of these systems the gas disks are likely to be gravitationally unstable, assuming entirely local formation and a standard gas-to-dust ratio. She concluded that planets or their building blocks at further distances were transported to the inner disk.

Here we consider two scenarios that could explain the origin of super-Earth planets. The disk migration scenario (Terquem & Papaloizou 2007; McNeil & Nelson 2010; Wang & Ji 2014; Cossou et al. 2014; Coleman & Nelson 2014, 2016; Ogihara et al. 2015; Liu et al. 2015, 2016; Izidoro et al. 2017; Ormel et al. 2017) assumes that (proto)planets have already formed in the outer part of the disk. They then undergo inward Type I migration (see Kley & Nelson 2012, for a review) until reach the inner disk edge, where the stellar magnetic field truncates the disk (Lin et al. 1996). On the other hand, the in-situ scenario assumes that super-Earths form in the inner part of the disk without (substantial) disk migration (Hansen & Murray 2012, 2013; Lee et al. 2014; Dawson et al. 2016). Importantly, we would like to emphasize that our definition of in-situ formation allows for material to be brought in from the outer disk, in the form of pebbles (Weidenschilling 1977a) or planetesimals (Grishin & Perets 2015). These drifting pebbles stop and accumulate at pressure bumps in the inner disk region (Chatterjee & Tan 2014; Hu et al. 2016). Such a large concentration of solids can therefore trigger streaming instability to generate planetesimals (Youdin & Goodman 2005; Johansen et al. 2007). Subsequent cohesive collisions among planetesimals yield the super-Earth planets. One of the goals in this paper is to investigate whether we can discriminate between the *in situ* and migration scenarios (also see Ogihara et al. 2015; Lee & Chiang 2017).

In Liu et al. (2017, referred to as Paper I hereafter), we proposed a new mechanism – magnetospheric rebound – which can rearrange the dynamical configuration of super-Earths during the gas disk dispersal phase. We constructed a disk model with an inner magnetospheric cavity, which expands during disk dispersal. The Type I torque that the planet experiences is negative when the planet is far away from the cavity radius. But the torque becomes positive near the cavity radius, which stalls the inward migration. Adopting analytical expressions of the Type I torque, we conducted *N*-body simulations on the evolution of two-planet systems. As the disk gas depletes, the planets migrate outward with the cavity expansion. When planets decouple from the cavity radius, they end up in a non-resonant configuration. As one of our key results, we found that our model predicts a correlation between the period ratio of two planets and their mass ratio.

In this work (Paper II) we will study the consequences of the magnetospheric rebound model for the above two super-Earth formation scenarios. The paper is structured as follows. In Sect. 2, we briefly review our model in Paper I, and then outline the initial conditions of the two formation scenarios. For both scenarios we statistically simulate the evolution of the *Kepler* two-planet systems during the gas-disk depletion (Sect. 3). In Sect. 4, we compare our model results with the observations by investigating different distributions of input parameters. We summarize our findings in Sect. 5.

2. Model

2.1. Model description

We briefly discuss the magnetospheric rebound model, which is described in detail in Paper I. The magnetospheric cavity

truncates the disk at a radius,

$$r_{\rm c} = 0.1 \left(\frac{\dot{M}_{\rm g}}{10^{-9}~M_\odot~{\rm yr}^{-1}} \right)^{-2/7} \left(\frac{B_*}{1~{\rm kG}} \right)^{4/7}~{\rm AU}, \tag{1}$$

where $\dot{M}_{\rm g}$ is the gas disk accretion rate and B_* is the stellar magnetic field strength at the stellar surface. The disk is assumed to be in a steady state such that the relation between the gas surface density Σ and $\dot{M}_{\rm g}$ reads

$$\dot{M}_{\rm g} = 3\pi\Sigma\alpha_\nu, \tag{2}$$

where α_ν is the dimensionless viscous parameter (Shakura & Sunyaev 1973). We assume that the disk remains accreting at a constant rate during the gas-rich phase, but that $\dot{M}_{\rm g}$ declines exponentially with a depletion timescale ($\tau_{\rm d}$) after a time τ_0:

$$\dot{M}_{\rm g} = \begin{cases} \dot{M}_{\rm g0} & \text{when } t \le \tau_0; \\ \dot{M}_{\rm g0} \exp\left[-(t - \tau_0)/\tau_{\rm d} \right] & \text{when } t > \tau_0. \end{cases} \tag{3}$$

Here, $\dot{M}_{\rm g0}$ refers to the initial disk accretion rate at the onset of disk dispersal.

The model contains three disk and stellar parameters: the initial gas disk accretion ($\dot{M}_{\rm g0}$), the disk dispersal timescale ($\tau_{\rm d}$), and the stellar magnetic filed strength (B_*). Following Paper I, we also assume $\alpha_\nu = 10^{-2}$. We note, however, that the model results are not restricted to the specific choice for α_ν. For instance, scaling by an arbitrary factor F, a new set of parameters can be formed as $\tilde{\alpha}_\nu = F\alpha_\nu$, $\tilde{\dot{M}}_{\rm g0} = F\dot{M}_{\rm g0}$ and $\tilde{B}_* = \sqrt{F}B_*$. It follows from Eqs. (1) and (2) that the results with this new set of parameters ($\dot{M}_{\rm g}$, $\tilde{\alpha}_\nu$, $\tilde{B}_*$) would be identical to those of ($\dot{M}_{\rm g}$, α_ν, B_*).

2.2. Formation scenarios of super-Earth planets: migration vs. in-situ

We investigate two formation scenarios for super-Earth planets: the migration scenario and the in situ scenario. These scenarios determine the initial periods (ratios) of the planets before disk dispersal. In Sects. 3 and 4, we then show how magnetospheric rebound operates for these two scenarios.

1. In the migration scenario super-Earths form in the outer part of the disk (e.g., at or beyond the snowline). After acquiring their masses, planets undergo Type I migration toward the inner edge of the disk. For simplicity, we adopt the local isothermal approximation for the Type I torque, and the migration is always inward (see Paper I). We also assume that the differential formation timescale of neighboring planets is longer than their migration timescale. Therefore, the inner planet has already migrated to the inner disk edge ($r_{\rm c}$) before the outer planet starts migration. While migrating, the outer planet is able to cross higher-order resonances easily (e.g., 3:1 mean motion resonance (MMR), Quillen 2006). The 2:1 MMR is the first strong resonant barrier in which planets may get trapped. In the *N*-body simulation, we therefore initialize the inner planet at the inner disk edge and the outer planet at a period ratio of 2.1, just slightly out of their 2:1 MMR.
2. In the in-situ scenario super-Earths accrete solid materials in the inner disk region. These planetary building blocks could be planetesimals or pebbles that drifted from the outer part of the disk. Because the differential formation timescale of these low-mass planets is shorter compared to their migration timescale, we do not expect that embryos would undergo sufficient migration during rapid planetesimal accretion (Chiang & Laughlin 2013) or pebble accretion

(Ormel & Klahr 2010; Lambrechts & Johansen 2012). In the in situ case, the inner planet is initially assumed to be located at the disk edge, whereas the outer planet is separated randomly from six to ten mutual Hill radii, as a consequence of orbital repulsion (Kokubo & Ida 1998).

3. Fiducial case

We perform *N*-body simulations of two-planet systems. Apart from the stellar and planet gravitational forces, the planet-disk interaction is taken into account by adding Type I torques (see Paper I for details). We aim to investigate the evolution of the planets during the disk dispersal phase. While Paper I focused on mapping the architecture of individual *Kepler* systems, here we conduct a statistical comparison between the model outcomes and the observed *Kepler* population for the two formation scenarios (Sect. 2.2). Specifically, we assume that the key model parameters ($\dot{M}_{g0}$, τ_d and $B_\star$) are each log-uniformly (or uniformly) distributed between an upper and a lower limit. We also statistically clarify the influence of the model parameters.

3.1. Fiducial case set-up

The planetary systems are adopted from the *Kepler* "Q1-Q17 DR24" (Coughlin et al. 2016) data[1]. Here we select the sample based on the following criteria: (1) both confirmed planets and candidates with $R_p < 4 R_\oplus$; (2) only two-planet systems; and (3) solar-type host stars ($0.7 M_\odot < M_\star < 1.2 M_\odot$). This results in a sample of 318 planetary systems. These criteria are motivated by the main goal of our paper: to investigate whether the *Kepler* data can distinguish a preferred formation scenario in light of the magnetospheric rebound mechanism (see Sect. 4). The mechanism requires a non-gap opening condition, which is satisfied for low-mass planets around solar-type stars (see Sect. 5 of Paper I). So we restrict our sample by criteria (1) and (3). In this work, we focus on two-planet systems (criterion (2)) and their evolutions are only simulated during the gas disk dispersal phase. A two-planet system is always stable in a gas-free system when the planet's separation is larger than $2\sqrt{3}R_H$ (Hill stability; Gladman 1993). Our results show that two-planet systems are all Hill-stable towards the end of simulations. On the other hand, for systems with more than two planets a dynamical instability may be triggered after the depletion of disk gas. In that case, additional long-term dynamical evolution must be considered, which is beyond the scope of this work. We therefore restrict our sample to two-planet systems.

Since *Kepler* planets are detected by transit and only their radii are measured, we use Weiss & Marcy (2014)'s mass-radius relationship to obtain the planet masses:

$$\frac{M_p}{M_\oplus} = \begin{cases} 2.69(R_p/R_\oplus)^{0.93} & \text{when } R_p \geq 1.5 R_\oplus, \\ \rho_p/\rho_\oplus(R_p/R_\oplus)^3 & \text{when } R_p < 1.5 R_\oplus, \end{cases} \quad (4)$$

where $\rho_p = 2.43 + 3.39(R_p/R_\oplus)$.

The rapid disk depletion timescale (τ_0) in Eq. (3) is numerically set to be 10^4 yr. The first 10^4 yr simulation represents the gas-rich phase evolution when planets undergo inward migration and get trapped in a stable resonant state. As long as $\dot{M}_{g0}$ remains fixed, r_c will stay the same and the planets will keep their orbits. When the disk starts to disperse ($t > \tau_0$), however, planets migrate outward with the cavity. The simulation is terminated when

[1] http://exoplanetarchive.ipac.caltech.edu/index.html

$t = \tau_0 + 10\tau_d$ so that the gas density is 10 e-foldings of the initial value.

Each simulated system is assigned one specific set of initial disk and stellar *B*-field parameters ($\dot{M}_{g0}$, τ_d, $B_\star$). Since the early disk and stellar properties are not well constrained, we obtain them by random sampling from a distribution. The distribution that we consider in this section is referred to as the fiducial distribution D.1 (Table 1): the disk dispersal timescale (τ_d) is logarithmically sampled between 10^2 yr to 10^5 yr, the stellar *B*-field strength is linearly sampled between 0.3 to 3 kG, and the initial gas disk accretion rate is sampled logarithmically between $10^{-8} M_\odot$ yr^{-1} to $\dot{M}_{g,max}$ (see below).

Concerning the initial gas disk accretion rate ($\dot{M}_{g0}$), the minimum value corresponds to the typical value of young T Tauri stars, while the maximum value is a function of $B_\star$. Since the cavity radius (r_c) is a decreasing function of the disk accretion rate (Eq. (1)), r_c would be very close to the host star when $\dot{M}_{g0}$ is very high. The planets are at risk of being engulfed or tidally disrupted by their central stars. We therefore truncate the disk at 0.02 AU, twice the radius of the young star ($2 R_\star = 4 R_\odot$), which, from Eq. (1) corresponds to an accretion rate of

$$\dot{M}_{g,max} = 2.8 \times 10^{-7} \left(\frac{B_\star}{1 \text{ kG}}\right)^2 M_\odot \text{ yr}^{-1}. \quad (5)$$

The disk lifetime is a few Myr whereas the timescale of late stage disk dispersal is at least one order of magnitude shorter (Williams & Cieza 2011). Physically, the stellar UV and X-ray irradiation efficiently removes the disk gas by photo-evaporation, starting at around 1 AU from the central star (Alexander et al. 2006). We focus on the super-Earths in the inner disk where the gas is therefore drained quickly by viscous diffusion ($\sim 10^4$–10^5 yr for $\alpha = 10^{-2}$). In addition, disk winds could further reduce the depletion timescale (Suzuki et al. 2010). For simplicity, we only mimic the depletion of the gas disk by considering a range of τ_d, from 10^2 yr to 10^5 yr.

3.2. Period ratio distribution

In Fig. 1 we present the result of our simulations (fiducial case) in terms of the period ratio histogram. The upper and lower panel illustrate the migration and the in-situ scenario, respectively. Three distributions are shown: the observed *Kepler* systems (black), the distribution before disk dispersal (light), and the final distribution after disk dispersal (dark).

In Fig. 1a, the planets are assumed to have formed through the migration scenario. Initially, they start at a period ratio 2.1 (Sect. 2.2). After disk dispersal we find that nearly one third of the planets remain close to the 2:1 resonance. However, the rest of the planets undergo substantial migration. The rebound plays a crucial role during disk dispersal, which moves planets outward and increases their period ratios. Finally planets end up at period ratios over a wide range compared to their initial values.

In Fig. 1b planets are assumed to have formed through the in-situ scenario. Initially, they are separated by six to ten mutual Hill radii (approximately corresponding to period ratios between 1.1 to 1.4, see Sect. 2.2). The rebound also increases the period ratios of planets. We find that more planets end up inside the 2:1 resonance for the in-situ scenario than the migration scenario. Also, no strong resonance concentration is seen in the in-situ scenario.
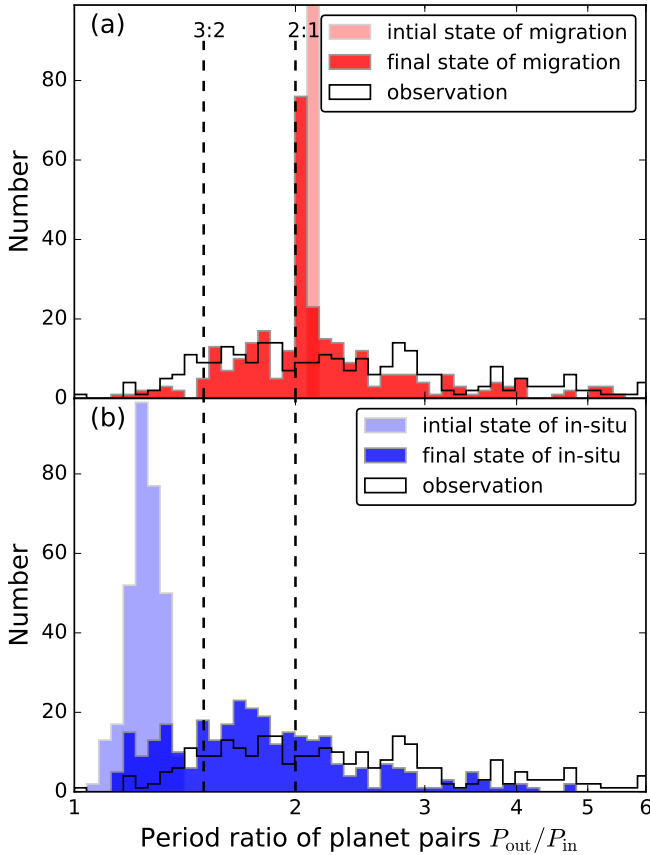
Fig. 1. Histogram of the outer-to-inner planet period ratio. The *upper* and *lower panel* show the results from the migration (red) and the in-situ (blue) scenario, respectively. In each scenario, both the initial (light) and final states (dark) of the simulations are given. The black line is the observation data for comparison. Vertical lines indicate the 2:1 and 3:2 MMRs.

3.3. Parameter dependence

3.3.1. Initial gas disk accretion

In Fig. 2 the results of the simulations are shown as a scatter plot of the inner planet period and the outer-to-inner planet period ratio. Three panels illustrate the dependence of these results on different parameters by colorbars.

In Fig. 2a, the color corresponds to the value of the initial gas disk accretion rate. We find that for the migration scenario, systems with high accretion rates are more frequently found inside the 2:1 resonance than those with low accretion rates. A large number of planets in low accretion disks (white) are clustered at period ratios $\gtrsim 2$, because they are trapped in 2:1 resonances in the early gas-rich phase. They also migrate modestly during disk dispersal and end up at period ratios around 2. On the other hand, planets in high accretion disks ($\gtrsim 2-3 \times 10^{-7} \, M_\odot \, \mathrm{yr}^{-1}$) are more likely to bypass the 2:1 resonance to end up in, for example, the 3:2 resonance. In addition, resonance trapping depends on planet mass. We find that systems with low-mass planets ($M_\mathrm{p} \simeq M_\oplus$) are able to bypass the 2:1 resonance even in low accretion disks, which is consistent with the analysis and simulations of Ogihara & Kobayashi (2013).

In the in-situ scenario planets are initially in a compact configuration (all planets are within the 3:2 MMR). In this case, we find that planets end up at a smaller period ratio in low accretion disks (white) than those in high accretion disks (orange). This

is because the rebound cannot efficiently move planets outward and increases their period ratios in low accretion disks.

The variation of the disk accretion rate has two consequences on the inner planet period. On the one hand, r_c truncates the disk further out when the disk accretion rate is lower, so the planet stops its inward migration at a larger distance from the star. On the other hand, planets cannot migrate outwards strongly due to weak rebound in low accretion disks. As a result, we do not find a clear dependence of the inner planet period on the disk accretion rate.

In conclusion, we find that for both scenarios planets in disks with a low accretion rate tend to stay in their original orbits. The period ratios show a wider distribution with increasing disk accretion rate, whereas the period distribution does not show a clear trend on the disk accretion rate.

3.3.2. Disk depletion timescale

In Fig. 2b we plot the same simulation result, but this time the color corresponds to the disk depletion timescale τ_d, which ranges from 10^2 to 10^5 yr. We find that the planets with a long depletion time (green) generally end up at longer periods and larger period ratios than those with a short depletion time (white). This behavior is simply due to the rapid depletion of gas, which limits the ability of the planet to migrate outwards. On the other hand, when the disk depletes slowly, both planets are able to migrate outwards, in sync with the cavity expansion, for a substantial time. The planet stops the outward migration when its migration timescale becomes longer than the depletion timescale (Sect. 3 of Paper I). As a result, systems with a short depletion timescale only rebound modestly while systems with a long depletion timescale can significantly expand their orbits.

3.3.3. Stellar *B*-field strength

In Fig. 2c we also examine the stellar *B*-field strength dependence on the final configuration of planetary systems. In general, we find that systems with large $B_\star$ (blue) end up at longer orbital periods. A larger stellar *B*-field truncates the disk at a larger cavity radius r_c (Eq. (1)). Therefore, the final period of the inner planet (P_in) becomes longer in systems with a stronger stellar magnetic field. However, the stellar magnetic field does not affect the period ratio of planets.

To summarize, the disk dispersal time affects both the inner planet period and the period ratio. In longer depletion disks planets migrate further out and end up at larger period ratios. The stellar magnetic field strength mainly determines the orbital period of the planet. Systems with stronger magnetic field strengths tend to have larger orbital periods. Planets in disks with low accretion rates tend to preserve their orbital configurations. Their period ratios can increase over a wide range as the disk accretion rate increases. These trends are independent of the planet formation scenario (initial condition).

4. Comparison to *Kepler* two-planet statistics

In this section, we focus on the comparison between simulations and observations. The observed data is selected from our *Kepler* sample, limited to two-planet systems (Sect. 3.1). Since the initial disk and stellar *B*-field parameters are poorly known, we have performed simulations for both the fiducial case (Sect. 4.1) and other underlying parameters' distributions (Sect. 4.2). Comparing the simulations to the observed periods and period ratios,
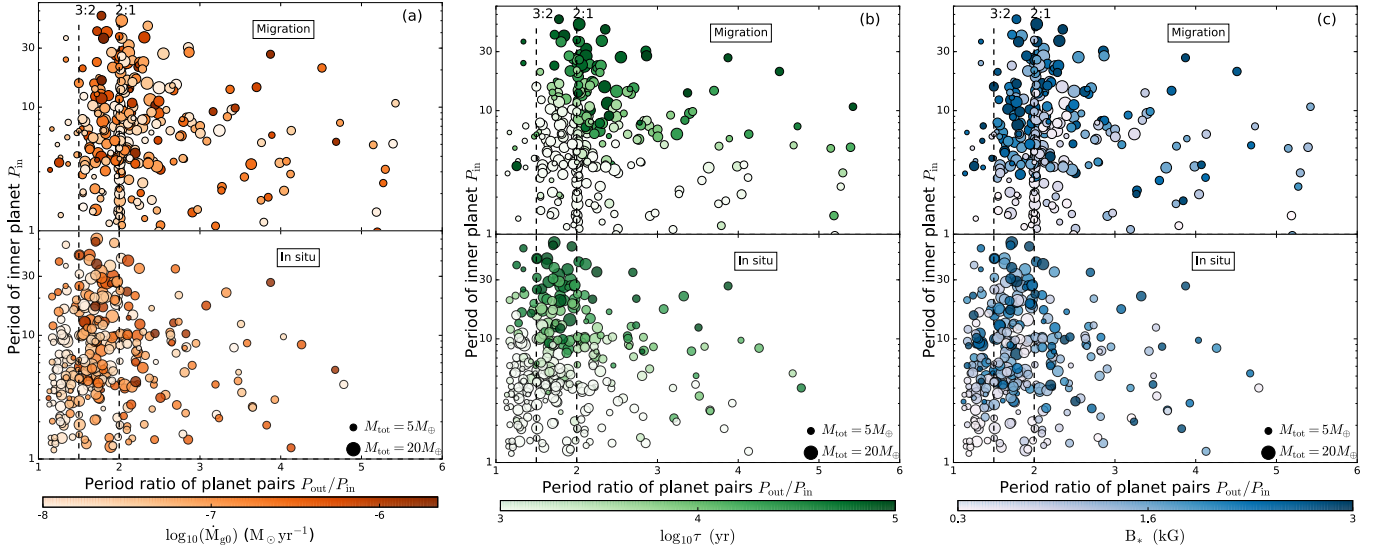
Fig. 2. Scatter plot of the inner planet period and the outer-to-inner planet period ratio. Each dot represents the final state of one particular planetary system. The color of the dot corresponds to $\dot{M}_{g0}$ (orange in *panel a*), τ_d (green in *panel b*), or $B_\star$ (blue in *panel c*), respectively. The size of the dot represents the total mass of two planets. Vertical lines mark the 2:1 and 3:2 MMRs.

we can infer which distribution and which scenario best fit the observations.

4.1. Fiducial case

4.1.1. Period ratio distribution

In Fig. 1 we have also plotted the observed period ratio of the *Kepler* sample (black open histograms). It can be seen that even though the initial period ratio distributions for the two scenarios are very different, magnetospheric rebound significantly reduces this disparity and results in two final period ratio distributions that are overall certainly similar to the observations. The clear exception is the 2:1 resonance excess in the migration scenario. We do not obtain a good match to the observations in that case. An additional mechanism to move the planet out of resonances is needed (see the discussion of Sect. 4.2).

4.1.2. Planet mass ratio

In Fig. 3, both simulation (upper) and observation (lower) are shown as a scatter plot of the inner planet period and the outer-to-inner planet period ratio. The color corresponds to the outer-to-inner planet mass ratio. A red (blue) dot indicates that the outer planet is more (less) massive than the inner planet.

The simulations (upper panel of Fig. 3) show that the planets' period ratio correlates with their mass ratio. In both scenarios, systems with larger outer-to-inner planet mass ratios (red) show a wide spread in period ratios. Conversely, systems with smaller outer-to-inner planet mass ratios (blue) have smaller period ratios. Specifically, in the migration scenario planets show a pile-up around the 2:1 MMR and a small fraction of the systems end up at period ratios smaller than 2. However, in the in-situ scenario, the dominant period ratio is smaller than 2.

Although the planets get trapped into resonance in the gas-rich phase, magnetospheric rebound rearranges the dynamical configuration of planets during disk dispersal. In the case of $M_{out}/M_{in} > 1$, the more massive outer planet is able to migrate outwards and decouple resonance when the inner planet falls into

the cavity. As a result, the rebound increases the planets' period ratio. However, in the case of $M_{out}/M_{in} < 1$, once the inner planet enters the cavity, the less massive outer planet cannot migrate outwards as fast as the expanding cavity. Thus, it also falls into the cavity and ends up at nearly resonant orbit with the inner planet. Therefore, with the rebound mechanism, the planets' period ratio correlates with the mass ratio of the planets.

Comparing simulations and observations (Fig. 3), the period ratio-mass ratio correlation shown by the simulations is not reflected in the observations, which, on first sight, do not exhibit any correlation between period ratio and mass ratio[1].

We propose several explanations for this discrepancy. First, both the observed and simulated distributions would be affected by any scatter and uncertainty that enters the conversion of *Kepler* radii into masses (Eq. (4)). It is, however, likely that the true mass will deviate from the estimated mass based on Eq. (4). For instance, Wolfgang et al. (2016) propose a probability model for the mass-radius relation rather than precise one-to-one mapping. Conceivably, many of the white dots ($M_{in} \simeq M_{out}$) shown in Fig. 3 could in fact be red. A better mass estimation or independent mass determination is needed to further verify our prediction. Second, some of the observed two-planet systems may have had more embryos at an early stage. After disk dispersal, planet scattering and mergers could produce a system with two planets or multiple planets with only the inner two close enough to be detectable. Systems that have experienced such a post-dispersal instability could have their period ratio–mass ratio correlation erased, due to the chaotic nature of the scattering. Finally, the magnetospheric rebound mechanism may not have operated because requirements have not been fulfilled (Paper I). For example, the well-ionized inner disk condition may not be true for some *Kepler* systems during their early evolution stage. Unfortunately, it is hard to presently assess which *Kepler* systems were most conducive for the rebound effect and those that were not.

---

[1] In order to determine whether such correlation exist in the data, a proper bias correction needs to be conducted (Steffen & Hwang 2015; Christiansen et al. 2015), which is beyond the scope of this work.
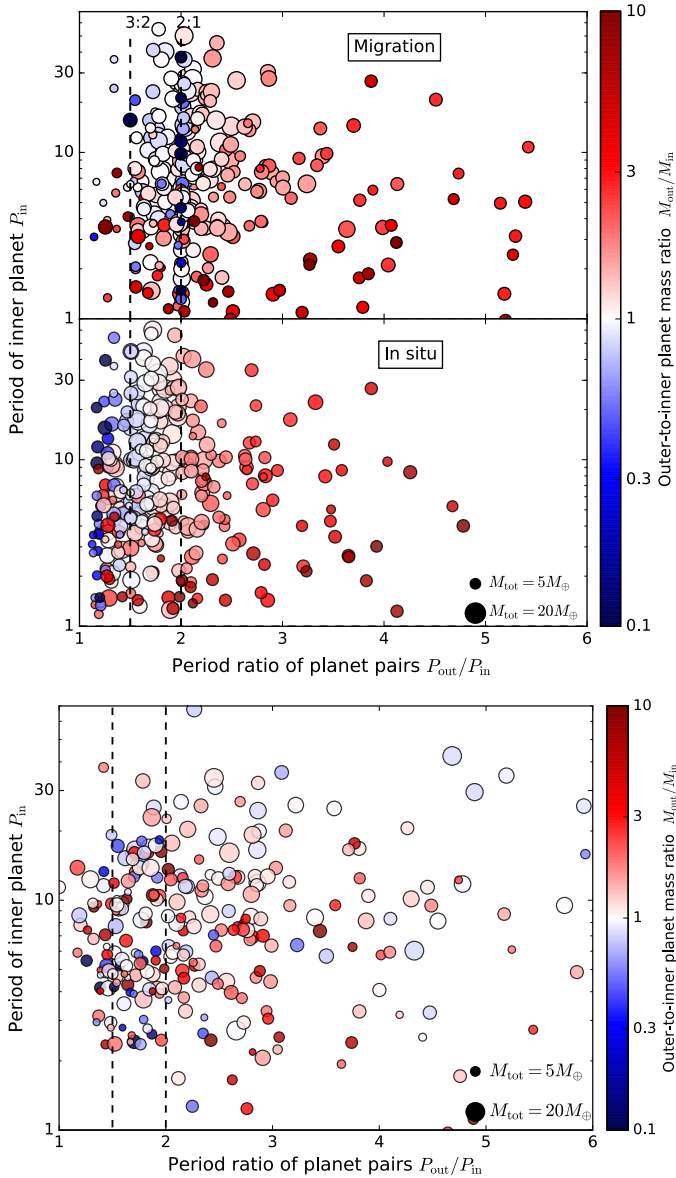
Fig. 3. Scatter plot of the inner planet period and the outer-to-inner period ratio from simulations (*upper panel*) and from our *Kepler* sample (*lower panel*). The size of the dot indicates the total mass of planets in an individual system, and the color (blue to red) corresponds to their outer-to-inner mass ratio (small to large). The masses of planets are calculated from their radii by Weiss & Marcy (2014).

4.2. Effect of different input distributions

In Sect. 4.1 we have only explored one particular distribution (D1 in Table 1). Here we study two additional distributions (D2-3 in Table 1), where D2 and D3 represent new simulations with different distributions for $\dot{M}_{g0}$ and τ_d, respectively. The "low disk accretion rate" runs (D2) feature a reduction of the minimum disk accretion rate by a factor of 10 (($\dot{M}_{g0,min} = 10^{-9}\ M_\odot\ yr^{-1}$) compared to the fiducial runs (D1) . Similarly, D3 and D1 have an identical distribution for the disk accretion rate, but the distribution for the disk depletion timescale is narrower and skewed towards large τ_d in D3, which ranges from 10^4 to 10^5 yr.

The results are shown in Fig. 4 as cumulative distributions for the inner planet period and period ratios, respectively. For the migration scenario (red curves), we find that less planets end up at period ratios smaller than 2 in the low accretion distribution

runs (D2) than in the fiducial case (D1) (Fig. 4a). This is because planets in low accretion systems cannot easily bypass the 2:1 resonance (Sect. 3.3.1). Hence, a lower disk accretion rate results in even more planets ending up at the 2:1 resonance, deteriorating the fit to the observations. For the in-situ (blue curves) scenario, more planets stay at short period ratios in D2, which also deteriorates the match to the observations. Because the magnetospheric rebound becomes weaker in a lower accretion disk, the period ratio of planets thus cannot increase much.

In Fig. 4b, we find that planets in the low accretion runs (D2) have an inner planet period distribution that is similar to the fiducial runs (D1). The cavity radius (r_c) becomes larger when $\dot{M}_{g0}$ is lower. However, rebound also becomes weaker when $\dot{M}_{g0}$ is lower. Combining these two effects, we find that the inner planet period distribution is almost unaffected by $\dot{M}_{g0,min}$ and that both runs fit the observed P_{inn} well.

Given our finding that a lower $\dot{M}_{g0,min}$ results in a worse fit to the period ratio distribution, the reader may wonder whether a larger $\dot{M}_{g0,min}$ would improve the fit to the observations. We adopt the minimum value of the disk accretion rate in the fiducial runs, $\dot{M}_{g0,min} = 10^{-8}\ M_\odot\ yr^{-1}$, for two reasons. First, it is the typical observed value among solar-mass, T Tauri stars. We do not expect systems to start their rapid disks dispersal at a very large $\dot{M}_{g0}$. Second, r_c is closer in when $\dot{M}_{g0}$ is larger (Eq. (1)). A larger $\dot{M}_{g0,min}$ results in the cavity radius close to the stellar truncation radius (0.02 AU), and the disk accretion rates are all close to the maximum value. We find this also does not improve the match to the observations.

Finally, we consider the comparison between the narrow τ_d distribution runs (D3) and the fiducial case (D1). The time τ_d represents how fast the disk gas depletes. A larger τ_d means that the disk depletes more slowly and that more gas is left to drive the planet migration and "fuel" the rebound. In Figs. 4c and d, we find that both the inner planet period and the planet period ratio are generally larger in the runs where the disk depletion timescales are longer (D3). As discussed in Sect. 3.3.2, rebound can move planets outwards when their migration timescale is shorter than the disk depletion timescale. Therefore, planets end up with larger period ratios in disks where the disk gas depletes more slowly. For the period ratio distribution (Fig. 4c), the simulations with the narrow τ_d distribution (D3) slightly improve the fit to the observations, both for the migration and the in situ scenario. However, in Fig. 4d we see that more planets in D3 end up at larger periods, which is inconsistent with the observations.

Optimizing the parameter distributions to obtain the best match to the observations is not the aim of this work. Instead, we have mainly focused on the general trends seen in the simulations and their implications in light of the magnetospheric rebound model. For the investigated parameter distributions, we find that neither scenario can perfectly explain the observational features. The main shortcoming of the in-situ scenario is that planets do not end up at very large period ratios (Fig. 1b). It is important to note, however, that we only consider two-planet systems. More embryos that form early could undergo giant impacts in the gas-free phase after the termination of the magnetospheric rebound. This chaotic process can reduce the number of planets by collisions, and increase their final separations (Hansen & Murray 2012, 2013; Pu & Wu 2015). Widely-separated planet pairs may form in this way. On the other hand, the problem with the migration scenario is that it produces an over-abundant population of planets at the 2:1 resonance. Additional mechanisms, such as stellar tides (Lithwick & Wu 2012; Delisle & Laskar 2014), stochastic disk

Table 1. Statistical survey.

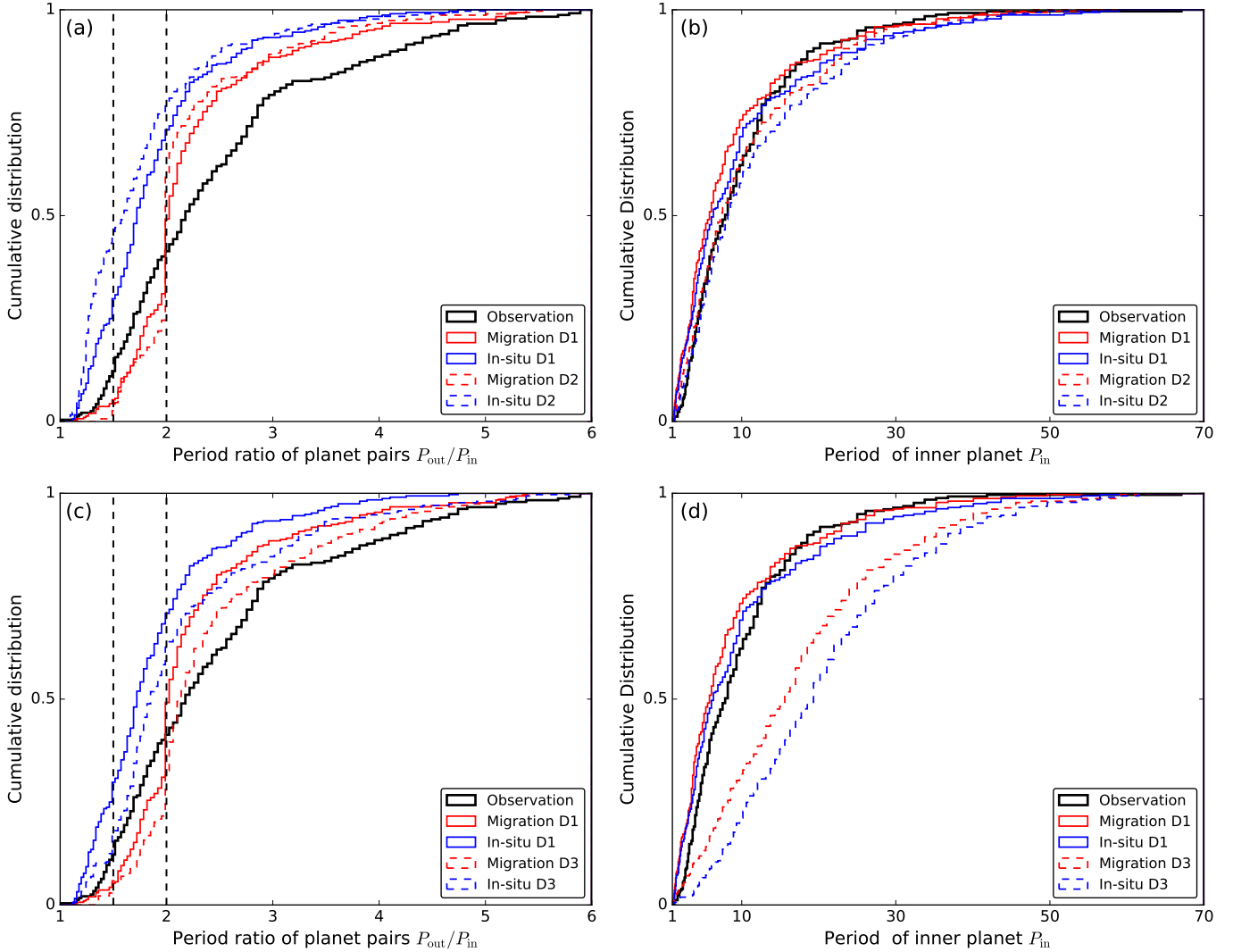| Distribution ID	Description	$\dot{M}_{g0}$ ($M_\odot$ yr)	τ_d (yr)	B_* (kG)
D1	fiducial	$[10^{-8}, \dot{M}_{g0,max}]$	$[10^2, 10^5]$	$[0.3, 3.0]$
D2	low disk accretion rate	$[10^{-9}, \dot{M}_{g0,max}]$	$[10^2, 10^5]$	$[0.3, 3.0]$
D3	long disk decay time	$[10^{-8}, \dot{M}_{g0,max}]$	$[10^4, 10^5]$	$[0.3, 3.0]$

Fig. 4. Cumulative distribution of planet period ratio (*left*) and inner planet period (*right*). The black solid line represents the observations, whereas the red and blue lines show the results from the migration and the in-situ scenarios, respectively. The solid lines are the result of D1 in *all four panels*. Dashed lines give the results of D2 in *panels a and b*, and D3 in *panels c and d*, respectively. Vertical lines mark the 3:2 and 2:1 MMRs.

torques (Rein 2012; Batygin & Adams 2017), or dynamical instabilities (Izidoro et al. 2017) are necessary to move planets out of resonances.

5. Conclusions

In this paper, we have investigated the magnetospheric rebound model that we introduced in Paper I in light of the *Kepler* data. We have studied the relation between the observed *Kepler* systems and modern planet formation theory from a statistical perspective. Two formation scenarios have been investigated – migration and in-situ – which result in different orbital properties in the early, gas-rich disk phase. We simulate the evolution of

the *Kepler* systems during the gas disk dispersal for these two scenarios. The influence of each model parameter ($\dot{M}_{g0}$, τ_d, and $B_\star$) on the inner planet period and period ratio distributions has been statistically investigated (Sect. 3). We have explored different sets of initial disk and stellar *B*-field distributions. The comparison between simulations and the observations is conducted in Sect. 4.

The major findings of this paper are summarized as follows:

1. Planets in disks with low accretion rates do not much change their orbits after the disk dispersal. Period ratios can increase significantly as disk accretion rates increase (Fig. 2a).

2. The disk dispersal time affects both the planet period and the period ratio. Planets in disks with longer depletion timescales end up with larger orbital periods and period ratios (Fig. 2b).

3. The stellar magnetic field strength mainly determines the period of the planet. Systems with stronger stellar magnetic fields tend to have longer orbital periods (Fig. 2c).

4. The magnetic rebound model predicts a correlation between the period ratios of planets and their mass ratios: systems with more massive outer planets end up at large period ratios whereas those with lighter outer planets preferentially stay at small period ratios. However, present-day *Kepler* systems do not seem to exhibit such correlation (Fig. 3).

5. The migration scenario overproduces 2:1 resonance planets. However, planets are less dominated by resonances compared to the gas-rich disk phase. In the in-situ scenario, planets increase their orbital periods and end up at larger period ratios. But, compared to the observations, there is still a lack of planets with very large period ratios (Fig. 1).

6. Magnetospheric rebound significantly diminishes the erstwhile differences between the two formation models. Therefore, it is hard to conclude which formation model best fits the *Kepler* two super-Earth planet population (Figs. 1 and 4).

Overall, the magnetospheric rebound model provides an explanation for a mass ratio-period ratio dependence, for the significant decrease in the number of resonant planets, and provides a vehicle for planets at large orbital periods and period ratios. These model predictions qualitatively agree with the observations. Nevertheless, we also give explanations why our model does not always match the observations (Sect. 4.2). As mentioned, the model outcome depends on the masses of the planets and particularly on the mass ratio. The masses of most *Kepler* planets, however, are difficult to infer by follow-up radial velocity surveys since the host stars are too faint. Future space missions, such as Transiting Exoplanet Survey Satellite (TESS) and Planetary Transits and Oscillations of stars (PLATO), have the ability to detect planets down to Earth-size around nearby bright stars. For these bright planets, follow-up RV surveys will be able to measure the masses accurately. Consequently, TESS and PLATO will provide larger and more precise data sets to verify the trends predicted by the magnetospheric rebound model.

References

Alexander, R. D., Clarke, C. J., & Pringle, J. E. 2006, MNRAS, 369, 229
Andrews, S. M., Wilner, D. J., Hughes, A. M., Qi, C., & Dullemond, C. P. 2009, ApJ, 700, 1502
Batygin, K., & Adams, F. C. 2017, AJ, 153, 120
Bonfils, X., Delfosse, X., Udry, S., et al. 2013, A&A, 549, A109
Buchhave, L. A., Bizzarro, M., Latham, D. W., et al. 2014, Nature, 509, 593
Chatterjee, S., & Tan, J. C. 2014, ApJ, 780, 53
Chiang, E., & Laughlin, G. 2013, MNRAS, 431, 3444
Christiansen, J. L., Clarke, B. D., Burke, C. J., et al. 2015, ApJ, 810, 95
Coleman, G. A. L., & Nelson, R. P. 2014, MNRAS, 445, 479
Coleman, G. A. L., & Nelson, R. P. 2016, MNRAS, 457, 2480
Cossou, C., Raymond, S. N., Hersant, F., & Pierens, A. 2014, A&A, 569, A56
Coughlin, J. L., Mullally, F., Thompson, S. E., et al. 2016, ApJS, 224, 12
Dawson, R. I., Lee, E. J., & Chiang, E. 2016, ApJ, 822, 54
Delisle, J.-B., & Laskar, J. 2014, A&A, 570, L7
Fabrycky, D. C., Ford, E. B., Steffen, J. H., et al. 2012, ApJ, 750, 114
Fabrycky, D. C., Lissauer, J. J., Ragozzine, D., et al. 2014, ApJ, 790, 146
Fang, J., & Margot, J.-L. 2012, ApJ, 761, 92
Fressin, F., Torres, G., Charbonneau, D., et al. 2013, ApJ, 766, 81
Gladman, B. 1993, Icarus, 106, 247
Grishin, E., & Perets, H. B. 2015, ApJ, 811, 54
Hansen, B. M. S., & Murray, N. 2012, ApJ, 751, 158
Hansen, B. M. S., & Murray, N. 2013, ApJ, 775, 53
Hayashi, C. 1981, Prog. Theor. Phys. Suppl., 70, 35
Howard, A. W., Marcy, G. W., Bryson, S. T., et al. 2012, ApJS, 201, 15
Hu, X., Zhu, Z., Tan, J. C., & Chatterjee, S. 2016, ApJ, 816, 19
Inamdar, N. K., & Schlichting, H. E. 2015, MNRAS, 448, 1751
Izidoro, A., Ogihara, M., Raymond, S. N., et al. 2017, MNRAS, 470, 1750
Johansen, A., Oishi, J. S., Mac Low, M.-M., et al. 2007, Nature, 448, 1022
Johansen, A., Davies, M. B., Church, R. P., & Holmelin, V. 2012, ApJ, 758, 39
Kley, W., & Nelson, R. P. 2012, ARA&A, 50, 211
Kokubo, E., & Ida, S. 1998, Icarus, 131, 171
Lambrechts, M., & Johansen, A. 2012, A&A, 544, A32
Lee, E. J., & Chiang, E. 2017, ApJ, 842, 40
Lee, E. J., Chiang, E., & Ormel, C. W. 2014, ApJ, 797, 95
Lin, D. N. C., Bodenheimer, P., & Richardson, D. C. 1996, Nature, 380, 606
Lithwick, Y., & Wu, Y. 2012, ApJ, 756, L11
Lithwick, Y., Xie, J., & Wu, Y. 2012, ApJ, 761, 122
Liu, B., Zhang, X., Lin, D. N. C., & Aarseth, S. J. 2015, ApJ, 798, 62
Liu, B., Zhang, X., & Lin, D. N. C. 2016, ApJ, 823, 162
Liu, B., Ormel, C. W., & Lin, D. N. C. 2017, A&A, 601, A15 (Paper I)
Lopez, E. D., & Fortney, J. J. 2014, ApJ, 792, 1
Marcy, G. W., Isaacson, H., Howard, A. W., et al. 2014, ApJS, 210, 20
Mayor, M., Marmier, M., Lovis, C., et al. 2011, ArXiv e-prints [arXiv:1109.2497]
McNeil, D. S., & Nelson, R. P. 2010, MNRAS, 401, 1691
Morbidelli, A., & Raymond, S. N. 2016, J. Geophys. Res. Planets, 121, 1962
Mulders, G. D., Pascucci, I., & Apai, D. 2015, ApJ, 798, 112
Ogihara, M., & Kobayashi, H. 2013, ApJ, 775, 34
Ogihara, M., Morbidelli, A., & Guillot, T. 2015, A&A, 578, A36
Ormel, C. W., & Klahr, H. H. 2010, A&A, 520, A43
Ormel, C., Liu, B., & Schoonenberg, D. 2017, A&A, 604, A1
Petigura, E. A., Howard, A. W., & Marcy, G. W. 2013, Proc. Nat. Acad. Sci., 110, 19273
Pu, B., & Wu, Y. 2015, ApJ, 807, 44
Quillen, A. C. 2006, MNRAS, 365, 1367
Raymond, S. N., & Cossou, C. 2014, MNRAS, 440, L11
Raymond, S. N., Kokubo, E., Morbidelli, A., Morishima, R., & Walsh, K. J. 2014, in Protostars and Planets VI (University of Arizona Press), 595
Rein, H. 2012, MNRAS, 427, L21
Schlichting, H. E. 2014, ApJ, 795, L15
Shabram, M., Demory, B.-O., Cisewski, J., Ford, E. B., & Rogers, L. 2016, ApJ, 820, 93
Shakura, N. I., & Sunyaev, R. A. 1973, A&A, 24, 337
Steffen, J. H., & Hwang, J. A. 2015, MNRAS, 448, 1956
Suzuki, T. K., Muto, T., & Inutsuka, S.-I. 2010, ApJ, 718, 1289
Terquem, C., & Papaloizou, J. C. B. 2007, ApJ, 654, 1110
Van Eylen, V., & Albrecht, S. 2015, ApJ, 808, 126
Wang, J., & Fischer, D. A. 2015, AJ, 149, 14
Wang, S. & Ji, J. 2014, ApJ, 795, 85
Weidenschilling, S. J. 1977a, MNRAS, 180, 57
Weidenschilling, S. J. 1977b, Ap&SS, 51, 153
Weiss, L. M., & Marcy, G. W. 2014, ApJ, 783, L6
Williams, J. P., & Cieza, L. A. 2011, ARA&A, 49, 67
Winn, J. N., & Fabrycky, D. C. 2015, ARA&A, 53, 409
Wolfgang, A., Rogers, L. A., & Ford, E. B. 2016, ApJ, 825, 19
Xie, J.-W., Dong, S., Zhu, Z., et al. 2016, Proc. Nat. Acad. Sci., 113, 41
Youdin, A. N., & Goodman, J. 2005, ApJ, 620, 459